Rolling motion of a bead in a rapid water stream

Christophe Ancey
Cemagref, Division ETNA, Domaine Universitaire, Boîte Postale 76, 38402 Saint-Martin-d'Hères Cedex, France

Françoise Bigillon
2524 Hydrosystem Laboratory, 205 North Mathews Avenue, Urbana, Illinois 61801

Philippe Frey
Cemagref, Division ETNA, Domaine Universitaire, Boîte Postale 76, 38402 Saint-Martin-d'Hères Cedex, France

Rémi Ducret
Cemagref, Division ETNA, Domaine Universitaire, Boîte Postale 76, 38402 Saint-Martin-d'Hères Cedex, France
(Received 1 July 2002; published 28 January 2003)

This paper investigates the two-dimensional rolling motion of a single large particle in a shallow water stream down a steep rough bed from both an experimental and a theoretical point of view. The experiment is prototypal of sediment transport on sloping beds. Two theoretical models are presented. The first model uses the mean kinetic energy balance to deduce the average particle velocity and the bounds of the flow-rate range within which a rolling regime occurs. This range is found to be narrow, which means that the fully rolling regime is a marginal mode of transport between repose and saltation. In the second model, the particle state (resting, rolling, saltating) is considered as a random variable, whose evolution constitutes a jump Markov chain. This makes it possible to deduce the mean particle velocity as a function of the flow conditions without explicit mention of its state. The theoretical results are finally compared to the experimental data. The second model provides correct estimates of the particle velocity and the probability of finding the particle in a given state for various flow conditions (bead material, slope, and roughness).

DOI: 10.1103/PhysRevE.67.011303 PACS number(s): 45.50.−j, 47.85.−g, 92.10.Wa

I. INTRODUCTION

The transport of solid particles in a rapid fluid stream is common in nature and in many industrial applications. Typical examples include sediment transport in rivers and estuaries [1,2], sand drift in the desert [3], blowing snow, a chemical exchanger, etc. The particles are usually entrained from a bed, made up of loose sediment, as a result of the fluid action and maintained in suspension or in saltation. Alternatively, particles may be transported as a result of rolling and sliding along the bed, dragged by the fluid. This type of transport has so far often been considered as marginal and, therefore, except for studies in air [4,5] or in a quiescent fluid [6], there have been very few attempts to describe and quantify particle transport in the rolling regime in a fluid phase. There are, though, a number of circumstances in which rolling may play a considerable role: for instance, when the particles are too heavy for turbulence to maintain them in suspension or when they are subject to adhesive forces [7], they roll and slide along the underlying surface. The rolling regime is probably the key mechanism in the formation of paved gravel-bed streams [8].

The purpose of this study was to investigate the two-dimensional rolling motion of a spherical particle along a rough inclined bottom in a rapid water stream. This paper will begin by developing a simple model providing the mean particle velocity as a function of the mean fluid velocity together with the bounds of the range of the fluid flow rate for which a rolling regime occurs. We will demonstrate that these bounds are close, so that the mere existence of the fully rolling regime can be questioned. A more robust theory will then be presented. The state X_t of the particle at a time t is assumed to be a random variable with three possible values: resting, rolling, and saltating phases. Treating (X_t) as a Markov chain, the mean particle velocity and the probability of finding the particle in a rolling or saltating phase will be deduced. The remainder of the paper will be devoted for comparing the experimental data and the theoretical results. After presenting the experimental facility and procedure in Sec. III, the two theoretical models will be applied to the flow geometry used and the effect of varying the parameters (channel slope, roughness, bead material) on the experimental results will be examined to test the robustness of the models.

II. THEORETICAL ANALYSIS

We consider the two-dimensional motion of a spherical particle of radius a in motion on a bumpy line (see Fig. 1). The line consists of juxtaposed half cylinders of radius r. It can be inclined at an angle θ to the horizontal. In the following we use the ratio of radii, $\xi = a/r$. Here only bed roughness sizes of the order of the mobile bead radius or lower are considered, $\xi = O(1)$. Smooth beds ($\xi \gg 1$) will not be examined.

Over the bumpy line, the water flow is assumed to be uniform and steady. The flow depth and discharge (per unit width) are, respectively, h and q. The mean velocity $\overline{u_f}$ is computed as $\overline{u_f} = q/h$. Using an approximate turbulence model, the discharge equation can be expressed as follows:

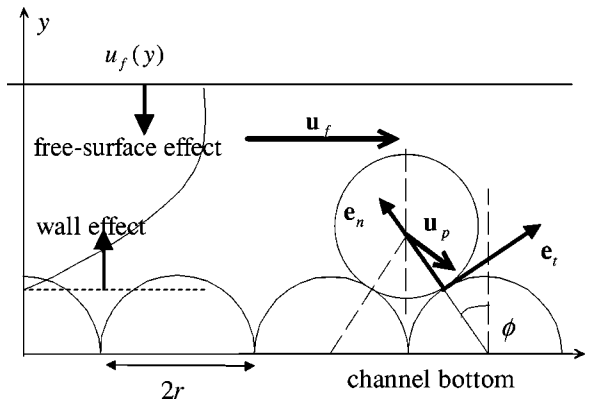

FIG. 1. Sketch of the physical system studied here.

$\overline{u_f}=C\sqrt{gh\sin\theta}$, where $C=\sqrt{8/f}$ is the Chézy coefficient, f is the Darcy-Weisbach coefficient ($f=0.223\ \mathrm{Re}^{-0.25}$ if we take the Blasius equation, where Re is the flow Reynolds number).

A. Approximate model

The mobile bead is considered in a Lagrangian system of coordinates. The coordinates in the streamwise and normal directions are denoted by x and y, respectively. The trajectory of the bead is assumed to be inscribed in a single plane (two-dimensional motion). The bead possesses three degrees of freedom. In the following, $\mathbf{u}_p=(u_p,v_p)$ denotes the instantaneous velocity of the mass center; the spinning velocity will be discarded since we will focus on the mean features of the motion. On average, for steady flow conditions, the energy supplied by gravity and fluid drag force is entirely dissipated by contact forces

$$m'g\sin\theta\overline{u_p}+\overline{P_D}=\overline{P_c}, \tag{1}$$

where the mean particle velocity defined as the time average velocity has been introduced: $\overline{\mathbf{u}_p}=\lim_{t\to\infty}\int_0^t\mathbf{u}_p(t')dt'/t$, $m'=m-4\pi\rho_f a^3/3$ is the buoyant mass, $\overline{P_D}=t^{-1}\int_t\mathbf{F}_D\cdot\mathbf{F}_p dt'$ is the power of drag forces supplied to the particle; the drag force is expressed as $\overline{F_D}=C_D(\mathrm{Re}_p)\pi a^2\rho_f|\overline{u_p}-\overline{u_s}|(\overline{u_p}-\overline{u_s})/2$, where $\overline{u_s}$ is the mean fluid velocity seen by the particle and the drag coefficient C_D has been expressed as a function of the particle Reynolds number $\mathrm{Re}_p=2a|\overline{u_p}-\overline{u_s}|/\nu$ with ν being the kinematic water viscosity. As a first approximation, we can consider that on average, $\overline{u_s}\approx\overline{u_f}$. The energy lost in contacts can be determined using the results obtained for a single bead rolling on a bumpy line in surrounding air. In this case, Ancey *et al.* [5] have shown that dissipation can be broken into frictional and collisional parts,

$$P_c=\lambda m'g\overline{u_p}\cos\theta+\alpha\frac{\chi}{2r}m\overline{u_p^3}, \tag{2}$$

where $(2r)^{-1}\chi\overline{u_p}$ is the collision rate (if the bottom beads are regularly and closely arranged, then $\chi=1$), $\alpha=0.063e^{4.96/(1+\xi)}$ reflects collisional dissipation and $\lambda=0.0025e^{7.46/(1+\xi)}$ is a bulk friction coefficient, weakly dependent on the Coulombic friction coefficient λ_p. The resulting equation of motion is a second-order polynomial of $\overline{u_p}$,

$$m'g\sin\theta+\varepsilon C_D\pi a^2\rho_f(\overline{u_p}-\overline{u_f})^2/2=\lambda m'g\cos\theta+\alpha\chi m\overline{u_p^2}/(2r), \tag{3}$$

where $\varepsilon=+1$ when $\overline{u_p}<\overline{u_f}$ and $\varepsilon=-1$ when $\overline{u_p}>\overline{u_f}$. The single physical solution is

$$\overline{u_p}=K(N_*)\overline{u_f}, \tag{4}$$

where the factor $K(N_*)$ is given by

$$K(N_*)=\frac{1-\sqrt{D}}{1-4\xi\alpha\Delta\rho\chi/(3\varepsilon C_D)}$$

in which we have introduced the density ratio $\Delta\rho=\rho_p/\rho_f$ and the discriminant $D=4\{4\xi\chi\alpha\Delta\rho\cos\theta(\tan\theta-\lambda)+3\varepsilon C_D[\alpha\Delta\rho\xi\chi N_*-\cos\theta(\tan\theta-\lambda)]\}/(9N_*C_D^2)$. The parameter $K(N_*)$ is expressed as a function of the dimensionless number N_*

$$N_*=\frac{\overline{u_f^2}}{2(\Delta\rho-1)ag}. \tag{5}$$

A helpful approximation can be proposed: at sufficiently large N_* values, the velocity tends to be independent of the slope and linearly proportional to the fluid velocity: $\overline{u_p}=K_\infty\overline{u_f}$ with $K_\infty=\lim_{N_*\to\infty}K(N_*)=[1+\sqrt{4\xi\alpha\Delta\rho\chi/(3C_D)}]^{-1}$.

The ratio N_* is very similar to the *Shields number* N_{Sh}, defined as the ratio of the bottom shear stress τ_b (shear stress exerted by the fluid at the channel base) to the equivalent in stress of a buoyant weight of the immersed particle: we have $N_{Sh}=N_*\tau_b/(\rho_f\overline{u_f^2})=fN_*/8$. The Shields number is a dimensionless number widely used in hydraulics to define the threshold of incipient motion [2,9]. The particle usually moves at a velocity lower than the fluid speed. However, for certain cases, the inverse situation cannot be excluded, for instance on steep slopes. According to Eq. (5), the condition $\overline{u_p}=\overline{u_f}$ ($\varepsilon=0$) yields $N_0=\cos\theta(\tan\theta-\lambda)/(\alpha\xi\chi\Delta\rho)$. When $N_*<N_0$, we have $\overline{u_p}<\overline{u_f}$ while for $N_*>N_0$, we have $\overline{u_p}>\overline{u_f}$; in that case, only gravity supplies energy to the particle while contact forces and water drag consume its energy. The latter condition holds only for slopes exceeding a critical value: $\theta>\theta_c=\arctan\lambda$.

From the previous analysis, it follows that three subregimes of motion can be considered in the rolling regime:

(1) For $\tan\theta<\lambda$, a solution is possible provided that the dimensionless number N_* exceeds a critical value equal to $N_{low}=4\cos\theta(\lambda-\tan\theta)/(3C_D)$; the value of N_{low} can be easily determined by equating $\overline{u_p}$ with zero in Eq. (3). In this subregime, motion mainly results from the water action.

(2) For $\tan\theta > \lambda$ and $N_* < N_0$, the single physical solution is given by Eq. (4) with $\varepsilon = -1$. Motion mainly results from the action of gravity. It is worth noting, however, that such a solution is usually unphysical, since the condition $N_* < N_0$ also implies $h < 2a$.

(3) For $\tan\theta > \lambda$ and $N_* > N_0$ the single physical solution is given by Eq. (4) with $\varepsilon = +1$. Motion mainly results from the combined action of water and gravity.

A more careful analysis shows that the bounds separating the flow regimes described above must be corrected:

(1) The upper bound corresponds to the transition from a rolling to a saltating regime. When $N_* \to \infty$, the particle reaches a large velocity and is more liable to liftoff from the bumpy line and jump. Indeed, during the rolling phase, whenever the rolling particle passes from one bottom cylinder to another, it experiences a collisional force that tends to eject it from the bottom. Fluid drag and gravity oppose this ejection and we can expect that, insofar as the particle velocity is low, this combined action is sufficient to dampen the normal impulse given to the particle. Let us quantify this dampening action by examining the resisting forces and the momentum exchange that occurs within a short time interval δt. The typical scale of the time step δt is the duration of an elastic collision, that is, $\delta t = 2.87\sqrt[5]{m^2/aE^2}/u_0^{3/5}$ [10], where E is the Young's modulus of the bead and u_0 denotes the instantaneous precollisional velocity. The components of the precollisional particle velocity are $u_0(\cos 2\phi, -\sin 2\phi)$ in the frame $(\mathbf{e}_t, \mathbf{e}_n)$, where $\phi = \arcsin[1/(1+\xi)]$ is the angle that the normal direction $\mathbf{e}_n$ makes with the direction normal to the channel base (see Fig. 1). Taking Maw's collisional law (see Ref. [11]), the components of the postcollisional velocities can be related to the precollisional velocity components as follows: $(u_t, \delta u) = u_0[\cos 2\phi + \lambda_p(1+e)\sin 2\phi, e\sin 2\phi]$, where λ_p denotes the Coulombic friction angle and e is the normal coefficient of restitution. Using this, we find that the momentum exchange in the normal direction is $\Delta p = mu_0(1+e)\sin 2\phi$. The projection of the combined action of gravity and water drag along the axis $\mathbf{e}_n$ is $m'g\cos(\theta - \phi) + F_{D,n}$, where $F_{D,n} = -\pi\rho_f a^2 C_D|\overline{u_f} - u_p|(\sin\phi\overline{u_f} - \delta u)/2$ is the normal component of the drag force. We can define the ratio of the resisting momentum to the collisional momentum exchange

$$R = \frac{\delta t(m'g\cos(\theta - \phi) + |F_{D,n}|)}{mu_0(1+e)\sin 2\phi}. \tag{6}$$

When $R \gg 1$, any takeoff is immediately dampened while, for $R < 1$, takeoff is a very probable event. In the latter case, the particle ceases to roll and begins a saltating motion. As exemplified in Fig. 2, the ratio R is a decreasing function of the fluid velocity. Somewhat arbitrarily, the limit between the saltating and rolling regimes can be considered to occur for R values close to unity. In that case, we define a critical number N_{up} and a critical fluid velocity u_{up} corresponding to the transition between the two regimes and computed by equating R with 1 in Eq. (6).

(2) The lower bound corresponds to the transition from a resting to a rolling regime. Following Wiberg and Smith [12] or Ling [13], if we assume that the particle at rest is submitted to a lift force F_L [with $F_L = C_L(Re_p)\pi a^2\rho_f|\overline{u_p} - \overline{u_f}|(\overline{u_p} - \overline{u_f})/2$] and drag force F_D in addition to its submerged weight $W' = 4\pi(\rho_p - \rho_f)ga^3/3$, the balance of moments provides the critical condition for incipient motion of spherical particles: $2\sqrt{2}F_D + F_L = W'$. If we assume that the mean velocity acting on the particle is $\overline{u_f}$, then we deduce that this condition can be put into the following dimensionless form:

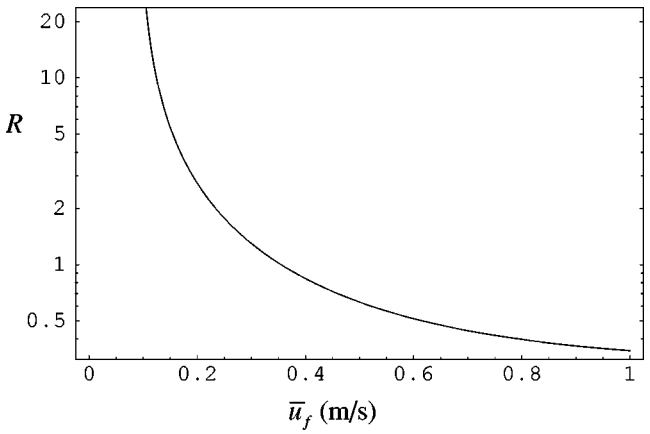

FIG. 2. Variation of the ratio R defined in Eq. (6) depending on the mean fluid velocity. Computation made for glass beads with $\phi = 30°$, $e = 0.85$, $C_D = 1$, and $\tan\theta = 0.05$.

$$N_{cr}(\theta = 0) = \frac{8}{12\sqrt{2}C_L + 6C_D}. \tag{7}$$

Extensions have been added to take into account the channel slope and the bed roughness. Chew and Parker [14] deduced that the critical Shields number at a given slope θ is linked to $N_{cr}(\theta) = N_{cr}(\theta = 0)\cos\theta(1 - \tan\theta/\tan\phi)$. When comparing N_{cr} and N_{low}, we find that $N_{cr} > N_{low}$, in accordance with common sense and experimental observations. Let us consider a particle in motion, that is, with a nonzero kinetic energy, and try to stop it (basically by dropping the water supply). Then, let us consider the opposite case of a bead initially at rest, trapped in a hole between two bottom cylinders, and try to set it in motion (basically by giving it a sufficient impulse or by increasing the water flow rate). Due to the difference in the initial kinetic energy, the critical conditions for the motion to cease and the conditions for initiating the motion do not coincide.

In short, we have to complete the motion diagram given above as follows: when $N_* < N_{low}$, there is no motion at all; when $N_{cr} > N_* > N_{low}$, the particle can roll or be at rest, depending on the flow conditions and its initial kinetic energy; for $N_{up} > N_* > N_{cr}$, the pure rolling motion occurs; for $N_* > N_{up}$, the particle is in saltation.

B. A more refined approach

A simple case study shows that the range of N_* for which a rolling motion occurs (the range $N_{low} - N_{up}$ according to the computations above) is narrow. Basically, with values from experiments (see below), we have found that N_{low}

≈ 0.5 and $N_{up} \approx 1$. According to this approximate model, different states can be reached by gently modifying the flow conditions. By averaging the energy balance equation, all sources of unsteadiness and fluctuations have been discarded. A typical example of this fluctuating environment is given by lift and drag forces, which vary significantly with time, because the fluid velocity fluctuates and fluctuating forces are induced by the interaction between the wake and the turbulent eddies shed asymmetrically into the wake [15]. Such fluctuations are sufficient to influence the rolling motion substantially. Consequently, even if our sole objective is to compute the mean velocity, we have to take into account the fluctuations of fluid velocity and forces. Since a complete treatment including turbulenct effects is far beyond our analytical capacity, computing the mean velocity requires considering the motion from a probabilistic viewpoint.

The motion can be described as a random sequence of resting, rolling, and/or saltating phases. At time t, the particle is in state i, with $i=1$, 2, or 3. Since the state at a given time depends only on the previous state, (X_t) constitutes a Markov chain with continuous time and three different states, here referred to as 1, 2, and 3, which represent the resting, rolling, and saltating states, respectively [16]. In the present case, the (transition) probability P_{ij} that the particle passes from state i to state j cannot easily be calculated, but we know that P_{ij} tends towards a constant stationary probability, interpreted as the limiting probability π_j that the chain is in state j independently of the initial state [16]. The stationary probability π_j is also the long-run proportion of time during which the particle is in state j; this property is useful since it will allow us to determine the stationary probabilities experimentally in a simple way: for a given run, if T_j denotes the time in which the particle is in state j, then we have on average, $\pi_j = T_j/(T_1+T_2+T_3)$.

An important property of Markov chains is that for any function h taking values on the state phase, we have the relationship [16]: $\lim_{t\to\infty} 1/n \Sigma_{i=1}^{t} h(X_i) = \Sigma_{j=1}^{3} \pi_j h(j)$. If $h(i)$ represents the mean particle velocity indexed on state i: $h(i) = \overline{u_p}$ when the particle is in state i, we have $h(1)=0$ and $h(2) = K(N_*)\overline{u_f}$ according to Eq. (4). For the saltating regime, it can be shown that the particle velocity is a fairly linear function of the mean velocity,

$$h(3) \approx A(\overline{u_f} - U_0), \tag{8}$$

where A and U_0 are two constants. Here we use the expression provided by Van Rijn for A and U_0 [17] (see also Ref. [18]). This makes it possible to provide a unified expression of the averaged particle velocity according to the mean fluid velocity,

$$\overline{u_p} = \pi_2(N_*, \theta) K(N_*) \overline{u_f} + \pi_3(N_*, \theta) A(\overline{u_f} - u_0). \tag{9}$$

The great advantage of this expression is that no explicit mention has been made of the motion regime. All the information on the state of the system is contained in the parameters π_2 and π_3, which now must be determined.

According to the previous deterministic analysis, the transition from state i to state j is described by a simple condition of the fluid velocity in the form $u_f > u_{crit}$, where $u_{crit} = u_{up}$ for the transition $2 \to 3$ (rolling to saltating) and $u_{crit} = u_{low}$ for the transition $1 \to 2$ (resting to rolling). Using experimental and theoretical results in the case of homogeneous turbulence [19] together with experimental data obtained in an open channel [20], we can assume as a first approximation that the probability density function of the fluid velocity $p_u(u_s|\overline{u_f}, \theta)$ tends to a Gaussian distribution: $p_u(u_s|\overline{u_f}, \theta) = e^{-(u_s-\overline{u_f})^2/(2\sigma^2)}/\sqrt{2\pi\sigma^2}$, where σ^2 is the fluid velocity variance. Therefore, from a probabilistic viewpoint, the probability that $u_f > u_{crit}$ is given by the probability of exceedance $1 - P_u(u_f|\overline{u_f}, \theta) = 1/2 - \mathrm{erf}((u_{crit} - \overline{u_f})/(\sqrt{2}\sigma))/2$. We then introduce $\psi_1 = 1 - P_u(u_{low}|\overline{u_f}, \theta)$, the exceedance probability associated with the transition $1 \to 2$ and $\psi_2 = 1 - P_u(u_{up}|\overline{u_f}, \theta)$, the exceedance probability associated with the transition $2 \to 3$. We obtain the stationary probabilities: $\pi_1 = 1 - \psi_1$, $\pi_2 = (1-\psi_2)\psi_1$, and $\pi_2 = \psi_2\psi_1$.

III. EXPERIMENTAL FACILITIES AND PROCEDURES

A. Particles

Two classes of spherical particles were used in the experiments: glass beads and steel beads. The particle density ρ_p was, respectively, 2500 and 7750 kg/m^3. Beads were calibrated particles whose nominal diameter $2a$ was 6 mm.

B. Channel

Experiments were carried out in a tilted, narrow, glass-sided channel, 2 m in length and 20 cm in height. The width W was adjusted precisely to be 1 mm larger than the particle diameter so that the particle motion was approximately two dimensional and stayed in the focal plane of the camera. Uncertainty on the width adjustment all along the channel was less than 2%. The channel inclination ranged from 0° to 20°, but in practice, the range was limited to 0°–12° because for steep slopes, the gravity waves (roll waves) traveled over the free surface of the water stream, which was therefore overly irregular. The channel slope could be adjusted very precisely using a screwjack, with uncertainty less than 0.1%.

The water supply at the channel entrance was controlled by an electromagnetic flow meter provided by Krohne (France). The discharge per unit width q ranged from 0 to 0.019 m^2/s. Uncertainty on the flow rate was less than 0.5%. Typically, this resulted in flow depths h and mean velocities $\overline{u_f} = q/h$ on the order of 0.02 m and 0.5 m/s, respectively; the flow depth was a few particle diameters. Most of the time, for channel slopes in excess of 1°, the water flow regime was supercritical, that is, the Froude number $\mathrm{Fr} = \overline{u_f}/\sqrt{gh}$ (where g denotes the gravity acceleration) exceeded unity. This also means that the water stream was fully controlled by the upstream condition on the water discharge; notably, the disturbances of the free surface caused by the particle could not move far upstream and affect the imposed flow rate.

The channel base was made up of regularly juxtaposed half cylinders of equal size. We also used random roughness, consisting of half cylinders of various sizes. Three sizes of cylinder were selected with a radius r of 1.5 mm, 3 mm, or 4 mm. Recall that we introduced the roughness parameter as the ratio of the bead radius to the roughness size $\xi = a/r$. In the present experimental setup, various disturbing effects arose. First of all, the relative roughness, i.e., the roughness size to the depth of flow ratio, was high, implying that the turbulence was substantially modified by the bottom. Moreover, the channel was narrow: the aspect ratio, defined as the width-to-depth ratio, was less than 5. This implies that the flow could also be substantially modified by the sidewalls. Last, flows were characterized by a low Reynolds number: indeed, the flow Reynolds number, computed as $\mathrm{Re} = 4R_H\overline{u_f}/\nu$, ranged from 2 000 to 10 000. In the Reynolds number definition, we introduced the hydraulic radius $R_H = Wh/(W+2h)$ and the water kinematic viscosity $\nu = \mu/\rho_f$ (where ρ_f is the water density and μ is the dynamic viscosity).

In order to verify the existence of a logarithmic velocity profile in the experimental channel, the velocity profile was measured in the direction normal to the bottom. To accomplish this, particle image velocity techniques were used: a vertical laser sheet was located at the channel centerline and filmed by a partial scan video camera Pulnix (progressive scan TM-6705AN). The flow was seeded with polyamide particles. We then applied an autocorrelation algorithm to twice-exposed images to obtain the velocity profile with uncertainty less than 5%. For the ranges of slopes and discharges tested here, we found that the velocity profiles systematically exhibited a logarithmic zone near the channel bottom. Depending on the discharge and channel slope, this zone extended up to $y/h = 0.3$–0.45. This value is to be compared to the usual value of $y/h \approx 0.2$ [20]. As shown in Fig. 3, the usual logarithmic law for hydraulically rough bottom fitted the data well,

$$\frac{u(y)}{u_*} = \frac{1}{\kappa}\ln\left(\frac{y}{k_s}\right) + B, \tag{10}$$

where u_* is the friction velocity (also called the shear velocity), $\kappa \approx 0.41$ is the van Kàrmàn constant, and $k_s = 4r/3$ is the equivalent size of the roughness. Parameter B was found to lie in the range 7.6–8.7 for $\xi = 1$, that is, close to the typical value of 8.5 given in the literature. Above the logarithmic zone, a blunt transition to a fairly flat profile was observed, as shown in Fig. 3.

In Fig. 3, the friction velocity was deduced experimentally by measuring the slope of the logarithmic part of the velocity profile, which should be equal to u_*/κ. We compared this value to the theoretical value $u_* = \sqrt{R_H g \sin\theta}$, which only holds for steady uniform flows in very large channels (i.e., when $R_H \approx h$). Since in the present case, the sidewalls were very smooth compared to the bottom, their influence on the discharge was limited. Thus, although the channel was narrow, the theoretical value $u_* = \sqrt{R_H g \sin\theta}$ provided a correct estimate of the friction velocity measured at the channel centerline. The relative deviation between the two values was less than 20%. The root mean square velocities were also measured in the streamwise and cross-stream direction, $u' = \sqrt{\overline{(u-\overline{u})^2}}$ and $v' = \sqrt{\overline{(v-\overline{v})^2}}$. We found that for $0.2 \leqslant y/h \leqslant 0.8$, the following scalings fitted the data well: $u' = 2.3u_* e^{-y/h}$ and $v' = 1.23u_* e^{-y/h}$, in agreement with empirical relationships given in the literature for open-channel flows [20]. It can be concluded that, despite the unusual features of our experimental device, the velocity profile and the main features of the turbulence are not too far from those typically observed in large channels.

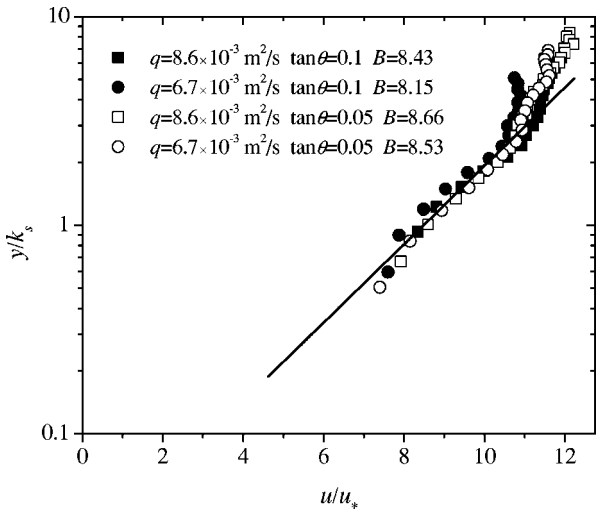

FIG. 3. Velocity profile of the water flow for different slopes and discharges. Measurements performed with a roughness made up of regularly spaced cylinders ($r = 1.5$ mm). The solid line represents the logarithmic profile fitted to the data: $u(y)/u_* = \kappa^{-1}\ln(y/k_s) + B$. The fitted value of B is tabulated on the figure caption.

In addition to the velocity profile, we determined the discharge equation, that is, the relationship between the flow depth and the flow rate. In practice, the flow depth was measured using either a rule placed against the sidewall or image processing and measuring the cross-stream distance between the top of the bottom half cylinders and the free surface. In both cases, uncertainty in the flow depth measurement was largely due to gravity and capillary waves along the free surface; typically, uncertainty on the flow depth measurement was within 0.5 mm. An empirical Darcy-Weisbach friction factor was fitted to the data (q, R_H) [21]. We obtained $q = \sqrt{8/f}h\sqrt{gR_H \sin\theta}$, in which $f = 0.6\ \mathrm{Re}^{-0.28}$, a form that is quite near to the Blasius equation used in open channel and pipe hydraulics ($f = 0.223\ \mathrm{Re}^{-0.25}$). The relative deviation between this fitted equation and data was less than 10%, except for large roughness ($r = 3$ mm), where the relative deviation exceeded 40%. From the Darcy-Weisbach equation, the approximate relationship between the mean and friction velocities can also be deduced, $u_* = \sqrt{f/8}\overline{u_f}$. The friction velocity u_* is a weakly nonlinear function of the mean velocity and, at high Reynolds numbers, we have $u_* \approx 0.08\overline{u_f}$.

The motion of the mobile bead was recorded using the Pulnix camera described above. Depending on the selected picture resolution, the frame rate ranged from 60 (resolution

of 640×480) to 220 frames per sec. (resolution of 640 ×100). Lights were positioned in the backside of the channel. An area of 20 cm in length and approximately 5 cm in height was filmed. Images were subsequently analyzed using the WIMA software provided by the *Traitement du Signal et Instrumentation* laboratory in Saint Etienne (France). The resulting uncertainty on the bead position was approximately 0.5 pixels. Typically, 50–200 images were required for each run to obtain a sufficiently long series of trajectories. The instantaneous particle velocity was computed as $\mathbf{u}_i(t) = (\mathbf{x}_{i+1} - \mathbf{x}_i)/\Delta t$, where Δt was the time between two consecutive frames. Uncertainty on the displacement of the bead between two frames was 1 pixel. To compute the instantaneous bead velocity, the minimum displacement used between two frames was 10 pixels. Thus the uncertainty on the instantaneous bead velocity had a maximum value of 10%. Mean particle velocities were obtained by measuring the time needed for the particle to cover the field filmed by the camera.

Complementary tests were performed to evaluate the fluid action on the particle. The first series of experiments was designed to estimate the value of the drag coefficient. It was expected that the usual values given in the literature (e.g., Ref. [22]) had to be modified to take into account the sidewall influence. The experiment involved dropping a particle in the horizontal channel filled with quiet water. The water depth was 10 cm. The vertical motion of the particle was filmed with the Pulnix camera. As soon as the particle reached a steady state, we measured the fall velocity w and we deduced the drag coefficient as follows: $C_D = 8(\Delta\rho - 1)ag/(3w^2)$. Experiments were performed with glass or steel beads of various diameters. These experimental values were found to be slightly larger than the experimental curve provided by Morsi and Alexander [22]. For instance, for a glass bead of 3 mm in diameter (corresponding particle Reynolds number $\mathrm{Re}_p = 870$), we found $C_D \approx 0.68$ while Morsi and Alexander's relationship gave $C_D \approx 0.52$; for a 3-mm steel bead (corresponding particle Reynolds number $\mathrm{Re}_p = 2200$), we found $C_D \approx 0.48$ while Morsi and Alexander's relationship gave $C_D \approx 0.42$. In the second series of experiments, the velocity profile of the water flow disturbed by the particle motion was measured. To our knowledge, very few experiments have been performed on this topic (see Morsi and Alexander [23] in their analysis of the velocity profile modification caused by a cylinder moving near a free surface). Figure 4 provides a typical velocity profile of the disturbed flow compared to the free flow and Fig. 5 shows a typical photograph of the velocity streams around the particle. The flow pattern surrounding the particle depends a great deal on the relative velocity of the particle and on its position relative to the free surface. For a particle in the middle position (Figs. 4 and 5), we observed that the particle induced a decrease in the local fluid velocity of the order of 20% in the wake zone while below and above the wake, the fluid velocity was increased by approximately 10%. A detailed analysis of the modification in the turbulent velocity field and turbulenct structures is outside the scope of the paper.

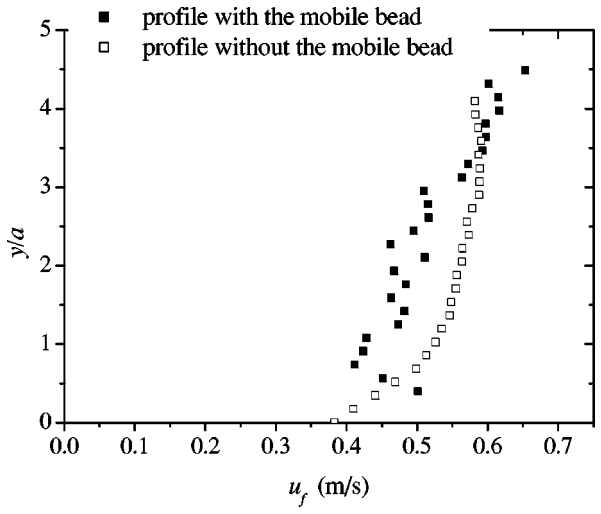

FIG. 4. Velocity profile of the water stream in the absence of the mobile bead or in its presence. Flow rate (per unit width) $q = 8.6 \times 10^{-3}$ m^2/s, channel slope $\tan\theta = 0.1$ ($\theta = 5.7°$), roughness ratio $\xi = 1$ (glass), bead radius $a = 3$ mm, channel width in 7 mm. The fluid velocity field around the particle is shown in Fig. 5.

C. Experimental procedure

A single particle was dropped from top into the water stream 1-m upstream from the measuring window. In order to avoid imparting a momentum to the dropped particle, we gently introduced it into the channel and a honeycomb cell at the channel entrance dampened its initial velocity. The motion of the particle was filmed with the Pulnix camera.

For each flow condition $(\overline{u_f}, \theta)$, variability of results was evaluated by repeating the run three to five times. In the following, only average values will be reported. Usually, the standard deviation was low relative to the mean (typically less than 5%) when the particle rolled, but when it is saltated, relative variations exceeding 15% were sometimes recorded between two similar runs. Though these mean velocities can-

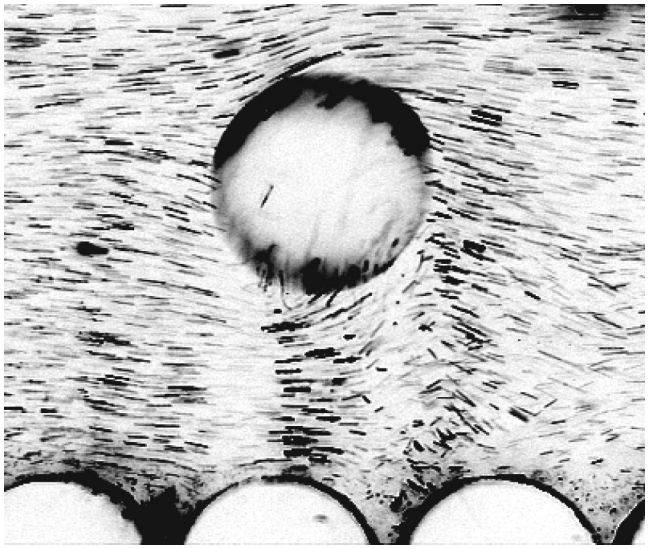

FIG. 5. Fluid velocity field around the particle for the flow conditions used in Fig. 5. The exposure time is 1/500 s.

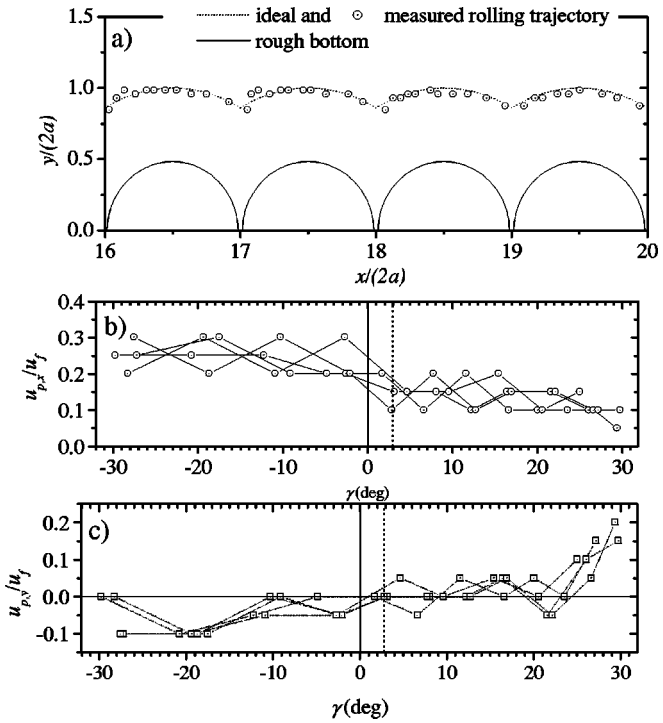

FIG. 6. (a) Typical rolling trajectory. (b) Downstream component of the bead velocity as a function of the angle γ that the particle mass center makes with respect to the normal to the bottom. $\gamma=0$ corresponds to the top of the cylinder and $\gamma>0$ corresponds to the ascending (upstream) part of the cylinder.(c) Normal component of the bead velocity as a function of γ. Experiment performed with $q=3.6\times10^{-3}$ m^2/s, $\tan\theta=0.05$, $h=8.2$ mm, $a=3$ mm, $r=3$ mm ($\xi=1$), and with a steel bead.

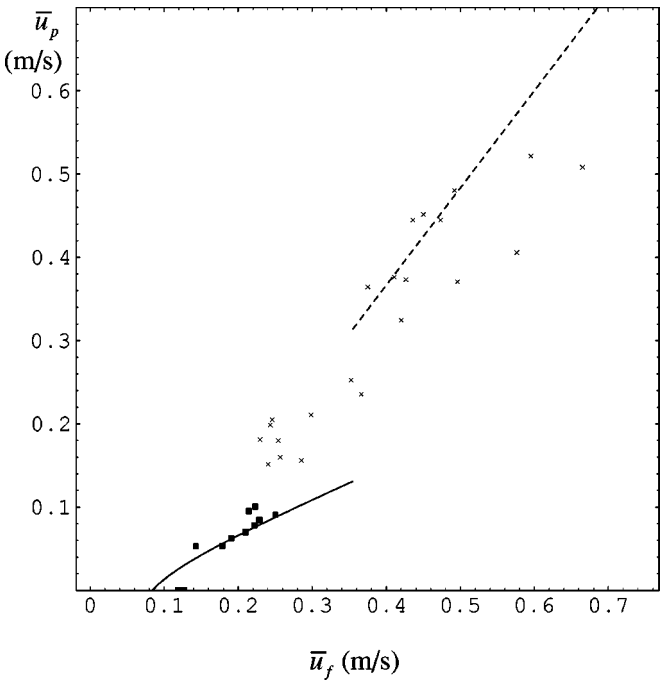

FIG. 7. Variation in the mean particle velocity as a function of the fluid velocity for the fully rolling regime (filled boxes) and the mixed regime (rolling+saltating: crosses). The bead was in glass. The experimental data obtained are $\tan\theta=5\%$, $a=3$ mm, $r=3$ mm. The continuous curve represents Eq. (4) while the dashed curve is given by $u_p=1.17(u_f-0.085)$, an equation proposed by van Rijn to model saltating particles.

not be rigorously assimilated to asymptotic velocities $\overline{u_p}$ (i.e., time-averaged values in the sense given in Sec. II A), they provide a reasonable approximation of $\overline{u_p}$.

We paid specific attention to two particular points. The first point concerns the precise definition of the rolling motion. Hereafter, the rolling motion refers to the motion of the bead in sustained contact with the bed; when colliding with a bed particle, the moving bead can undergo a microleap whose typical length is less than the bead radius a. Figure 6(a) shows a typical trajectory of the particle in a rolling regime: clearly the mass center of the particle follows a smooth periodic trajectory except when a collision occurs. In that case, a small leap can be seen. The second point concerns the deviations of the particle velocity from the mean velocity. As shown in Figs. 6(b),(c) for the two components of the particle velocity, the departures from the mean behavior were small, indicating that the particle reached a quasi-steady state. This means that a small number of runs (for given flow conditions) is usually sufficient to properly evaluate the average features of the motion of the rolling particle.

IV. EXPERIMENTS AND COMPARISON WITH THEORY

In the following, we will focus on two points: the mean particle velocity depending on the fluid velocity and the probability of finding the particle in a given state. Figure 7 shows the experimental relationship between the mean particle and fluid velocities for 6-mm glass beads (roughness of equal size, $\xi=1$ and $\chi=1$) and Fig. 8 gives the results for 6-mm steel beads (roughness of equal size, $\xi=1$ and $\chi=1$). The data used in both figures were obtained with a channel inclined at $\tan\theta=0.05$. Crosses represent data pertaining to a pure rolling regime while squares represent data where the particle motion was intermittent, combining rolling and saltating phases. Flow conditions for which the particle motion included a series of stopping and rolling phases were almost never observed (a few runs for steel beads and none for glass beads).

In the same figure (Fig. 7), the theoretical relationships providing the mean particle velocity as a function of the fluid velocity for glass beads are reported, computed using Eq. (4). It can be seen that the general trend provided by the approximate theoretical model is in agreement with experimental values. The range of fluid velocity for which a rolling regime occurs has also been reported. Numerically, taking $E=7000$ Pa, $C_D=1$, $e=0.85$, we found for glass beads of 6 mm in diameter: $u_{low}=0.08$ m/s ($N_{low}=0.08$), $u_{cr}=0.27$ m/s ($N_{cr}=0.85$), and $u_{up}=0.35$ m/s ($N_{up}=1.4$). The experimental critical fluid velocity corresponding to the beginning of motion was approximately 0.14 m/s (thus falling within the interval $u_{low}-u_{cr}$) while the critical velocity u_{up} was close to 0.24 m/s. As shown in Fig. 7, the approximate theoretical model yields the correct magnitude for the mean particle velocity and the bounds of the rolling regime.

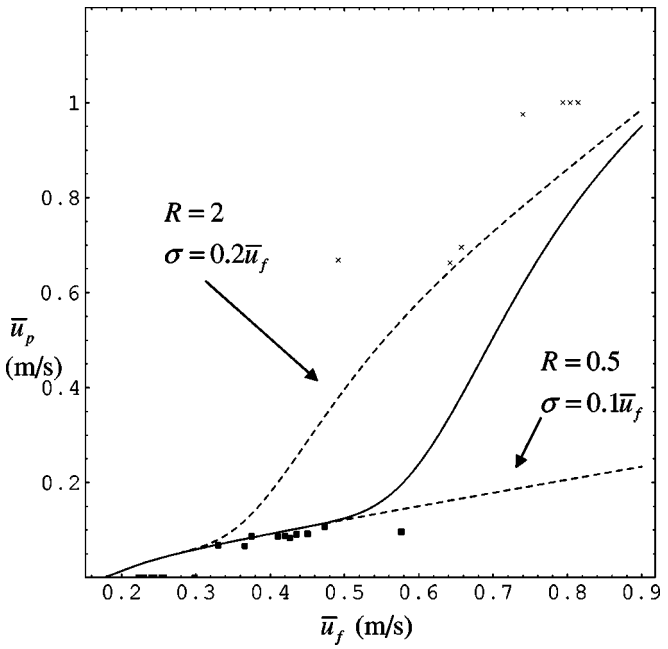

FIG. 8. Variation in the mean particle velocity as a function of the fluid velocity for the fully rolling regime (filled boxes) and the mixed (rolling+saltating) regime (crosses). The bead was in steel. The experimental data obtained are $\tan\theta=5\%$, $a=3$ mm, $r=3$ mm. The continuous curve represents the theoretical velocity given by Eq. (9) (calculated with a standard deviation $\sigma=0.15\overline{u_f}$ and $R=1$) while the dashed curves represent the same quantity, but computed with ($\sigma=0.1\overline{u_f}$, $R=1/2$) and ($\sigma=0.2\overline{u_f}$, $R=2$).

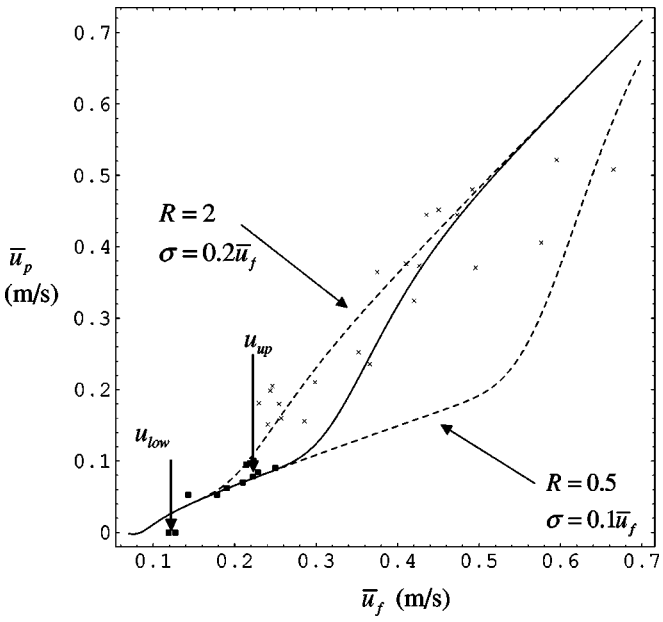

FIG. 9. Variation in the mean particle velocity as a function of the fluid velocity for the glass bead (same experimental data as Fig. 7). The continuous curve represents the theoretical velocity given by Eq. (9) (calculated with a standard deviation $\sigma=0.15\overline{u_f}$ and $R=1$) while the dashed curves represent the same quantity but computed with ($\sigma=0.1\overline{u_f}$, $R=1/2$) and ($\sigma=0.2\overline{u_f}$, $R=2$).The two arrows indicate the values found for u_{up} and u_{low}.

In Fig. 9, we have reported the phase-averaged particle velocity, computed using Eq. (9) and taking $\sigma=0.15\overline{u_f}$ for the standard deviation. The agreement seems better to the eye since the resulting curve smoothes out the brutal variations in particle velocity during phase changes. Due to the arbitrary choice made for the transitional velocity u_{up}, computed by setting $R=1$ in Eq. (6), and the standard deviation σ, which may substantially affect the stationary probability π_2, two other curves are reported in Fig. 9 in order to give an idea of the sensitivity of the model to the adjustment of its parameters. The first curve was obtained by taking $R=0.5$ and $\sigma=0.1\overline{u_f}$ in the stationary probability π_2; for the second curve we took $R=2$ and $\sigma=0.2\overline{u_f}$. As shown in Fig. 9, a better agreement was obtained with the second curve.

The same trend was observed with steel beads (see Fig. 8). For 6-mm steel beads, taking $E=2\times10^4$ Pa, $C_D=1$, $e=0.85$, we obtained $u_{low}=0.18$ m/s ($N_{low}=0.08$), $u_{cr}=0.57$ m/s ($N_{cr}=0.85$), and $u_{up}=0.68$ m/s ($N_{up}=1.19$). The experimental critical fluid velocity corresponding to the beginning of motion was approximately 0.31 m/s (still falling within the interval $u_{low}-u_{cr}$), while the critical velocity u_{up} was close to 0.6 ± 0.1 m/s.

In order to further test the refined model, the probability $P_{rolling}$ of finding the particle in a rolling regime depending on the dimensionless number N_* is reported in Fig. 10 for glass beads (see Fig. 11 for steel beads). For a given run, this probability was evaluated by dividing the time during which the particle rolled by the total time. The model predicts that the probability is given by $P_{rolling}=\pi_2(N_*,\theta)$. As previously, we added two dashed curves corresponding to the input parameters ($R=0.5$, $\sigma=0.1\overline{u_f}$) and ($R=2$, $\sigma=0.2\overline{u_f}$). The curves ($R=2$, $\sigma=0.2\overline{u_f}$) and ($R=1$, $\sigma=0.15\overline{u_f}$) give better results but with minor differences. The choice ($R=2$, $\sigma=0.2\overline{u_f}$) leads to a correct transition from the rolling to the saltating regime but underestimates the range of N_* for which a fully rolling regime occurred. In contrast, the

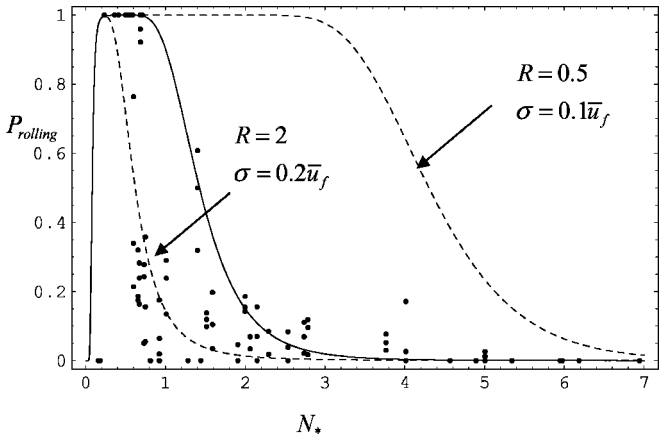

FIG. 10. The probability of finding the particle in a rolling regime (same experimental conditions as in Fig. 7) for a glass bead. The theoretical curve ($P_{rolling}=\pi_2$) is also reported with three values of its parameters. The continuous curve corresponds to ($\sigma=0.15\overline{u_f}$, $R=1$), while the dashed curves pertain to ($\sigma=0.1\overline{u_f}$, $R=1/2$) and ($\sigma=0.2\overline{u_f}$, $R=2$).

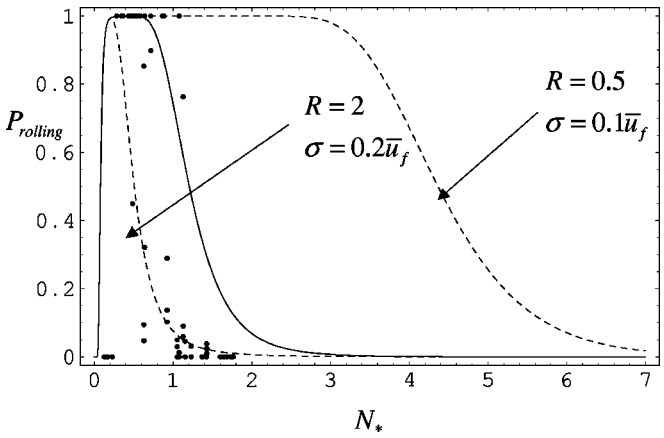

FIG. 11. The probability of finding the particle in a rolling regime (same experimental conditions as in Fig. 8) for a steel bead. The theoretical curve ($P_{rolling}=\pi_2$) is also reported with three values of its parameters. The continuous curve corresponds to ($\sigma=0.15\overline{u_f}$, $R=1$), while the dashed curves pertain to ($\sigma=0.1\overline{u_f}$, $R=1/2$) and ($\sigma=0.2\overline{u_f}$, $R=2$).

choice ($R=1$, $\sigma=0.15\overline{u_f}$) correctly predicted this range but slightly overestimated the probability $P_{rolling}$ in the transition from the rolling to the saltating regimes. The choice ($R=0.5$, $\sigma=0.1\overline{u_f}$) provided results in poor agreement with the experimental data. It can be concluded that with R chosen in the range 1–2, the model provides correct results as regards the particle velocity and the probability of finding the particle in a rolling regime. The same conclusion can be drawn for steel beads (see Fig. 11).

With the same objective in mind, we computed the probability of finding the particle in a saltating regime $P_{saltating}=\pi_3(N_*,\theta)$. The experimental data and theoretical curves are reported in Figs. 12 and 13 for glass and steel beads, respectively. As previously, for both materials we found that, provided R is chosen in the range 1–2, the theoretical model provides a correct estimate of $P_{saltating}$.

The predictions of the theoretical models were then tested when the channel slope or the roughness was changed. Limi-

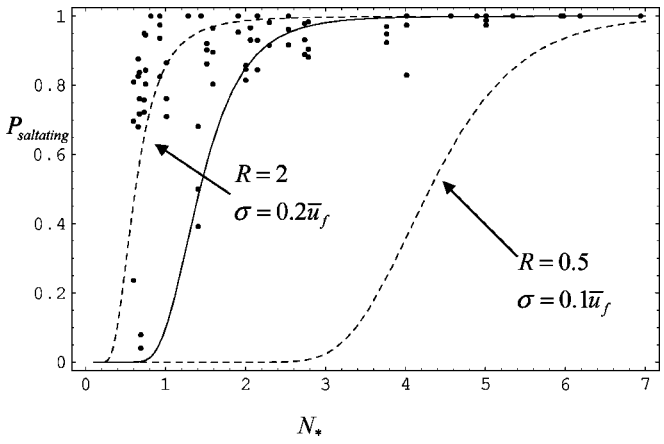

FIG. 12. The probability of finding the particle in a saltating regime for a glass bead. Same caption as in Fig. 9 except that the theoretical curves represent the $P_{saltating}=\pi_3$.

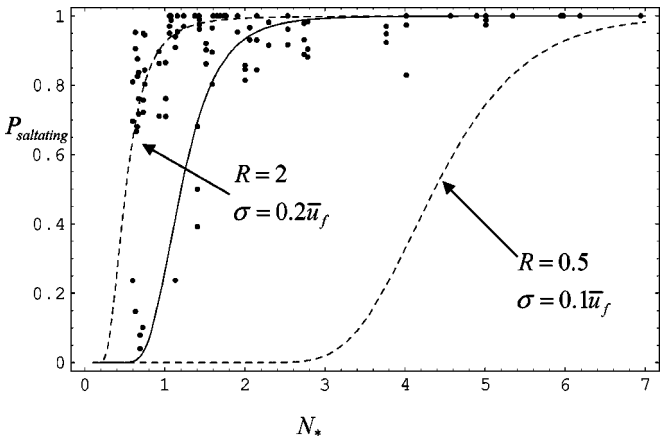

FIG. 13. The probability of finding the particle in a saltating regime for a steel bead. Same caption as in Fig. 9 except that the theoretical curves represent the $P_{saltating}=\pi_3$.

tations in the experimental facility made it impossible to explore a wide range of channel slopes when investigating the rolling motion. Indeed, when the channel slope was gentle (less than 1%), we could not supply a sufficiently high flow rate to set the particle in motion. Conversely, for high channel slopes, the water flow depth was rapidly too low for the particle to be immersed. Thus, in practice, at the very best (for steel beads) it was possible to explore narrow ranges of channel slopes (typically between 1 and 4) and flow rates, which made it difficult to make a detailed comparison between the experimental data and the theoretical results. Thus, only partial results are given in the following: notably, the model could not be tested as regards the dependence of the particle velocity on the channel slope. Figures 14 and 15 report the mean particle velocity depending on the mean fluid velocity and the probability $P_{rolling}$ depending on the dimensionless number N_* for different roughness ratios ξ. As shown in Fig. 14, the theoretical model provides correct estimates of the mean particle velocities even though the data scattering and the lack of data (notably for $\xi=3/4$) do not allow us to test the model more thoroughly. In contrast, although the model provides the correct trend for the effect of the roughness ratio on the probability of finding the particle in a rolling regime, it substantially overestimates the range over which the fully rolling regime occurs.

V. CONCLUDING REMARKS

We have presented two theoretical models to compute the mean velocity of a particle rolling down a bumpy bottom as a result of gravity and water drag. In the first model, the kinetic energy balance equation was used to determine the mean particle velocity as a function of the fluid velocity together with the bounds of the fluid velocity within which a rolling regime occurs. We found that this range was narrow, leading to the conclusion that the rolling regime is a marginal transport process between the resting and saltation phases. This also means that, for more irregular rough beds, the proposed model is not robust because the rolling regime occurs intermittently and not in a continuous way, as studied here. A

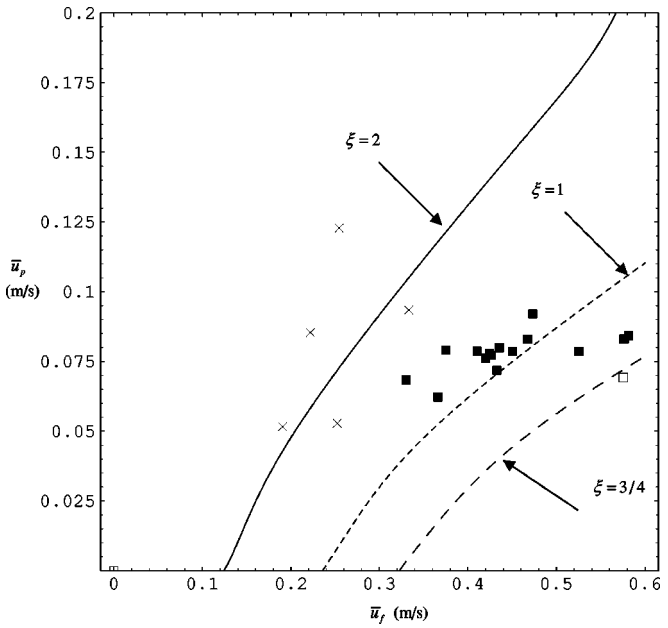

FIG. 14. Variation in the mean particle velocity as a function of the fluid velocity for the steel bead and three different roughness ratios and slopes. Crosses and continuous curve, $\xi=2$, $\tan\theta=0.02$; filled boxes and dashed curve, $\xi=1$, $\tan\theta=0.05$; open boxes and long dashed curve, $\xi=3/4$, $\tan\theta=0.075$. The curves represent the theoretical velocity given by Eq. (9) (calculated with a standard deviation $\sigma=0.15\overline{u_f}$ and $R=1$).

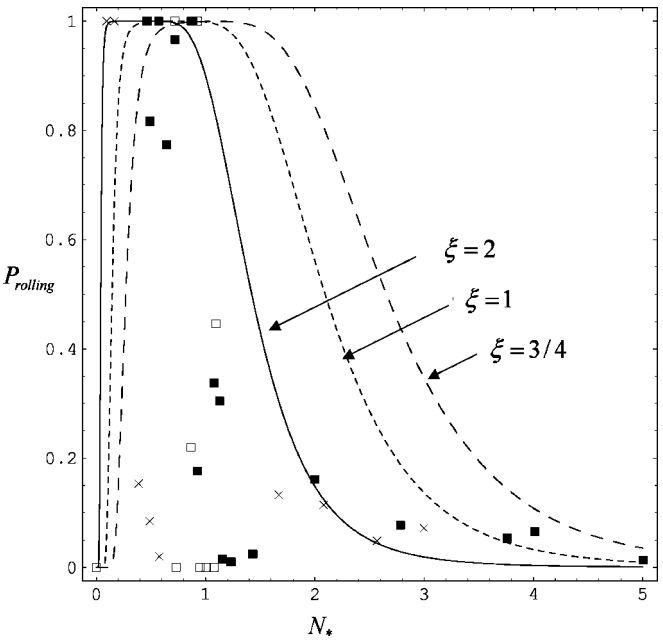

FIG. 15. The probability of finding the particle in a rolling regime (same experimental conditions as in Fig. 14) for a steel bead and for three different roughness ratios and slopes. Crosses and continuous curve, $\xi=2$, $\tan\theta=0.02$; filled boxes and dashed curve, $\xi=1$, $\tan\theta=0.05$; open boxes and long dashed curve, $\xi=3/4$, $\tan\theta=0.075$.

second model was then developed. The particle state (resting, rolling, saltating) was considered as a random variable whose evolution constitutes a jump Markov chain. In this way, using asymptotic properties of a Markov chain, we can infer the mean particle velocity without the explicit mention of its state. The model also provides the probability of finding the particle in a given state or passing from one state to another. Simple arguments without tuning parameters were used.

Careful experiments were performed to test the robustness of the models. The simple model is sufficient to provide the fairly good estimates of the particle velocity and the bounds of the rolling regime. The predictions of the stochastic model, as regards the probabilities of finding the particle in a given state and the particle velocity, are in good agreement with experimental data for a fairly wide range of flow conditions. In an approach to describing sediment transport in a microstructural framework, the second model appears to be a good candidate for generalization.

These experiments bring to mind the pioneering work of Hans A. Einstein, nephew of Albert, who proposed the first elements of a probabilistic theory of sediment transport in the 1950s (see Ref. [24] for an outline of his work). Eclipsed for several decades by the mean-field theory proposed by Bagnold [25], the ideas expressed by Einstein are today revisited with interest and there is a growing number of papers focusing on stochastic aspects of bed load transport. Punctual progress has been made in the examination of motion threshold [26] or the bed elevation variation [27] or, more generally, in the formulation of equations for two-phase turbulent flows [28], but a complete theoretical framework for modeling sediment transport (transport, erosion, and deposition) is still lacking. The next step in that direction is to experimentally examine the collective motion of beads in the same experimental device.

ACKNOWLEDGMENTS

This study was supported by the Cemagref and funding was provided by *Contrat Plan Etat-Région, Programme Avenir* of Rhône Alpes Région and by the *Programme national risque naturels* of INSU/CNRS, and *Action Concertée Incitative* ''Risques naturels'' of the CNRS, directed by P. Gondret. We are grateful to the laboratories TSI (Christophe Ducottet, Jacques Jay, and Jean-Paul Schon) and LCPC (François Chevoir) for their help.

[1] N.J. Balmforth and A. Provenzalle, in *Geomorphological Fluid Mechanics* edited by N.J. Balmforth and A. Provenzalle (Springer Verlag, Berlin, 2001), p. 369; Y.S. Yalin, *River Mechanics* (Pergamon Press, Oxford, 1992), p. 220.

[2] P. -Y. Julien, *Erosion and Sedimentation* (Cambridge University Press, Cambridge, 1994), p. 280.

[3] H. Tsoar, in *Geomorphological Fluid Mechanics*, edited by N.J. Balmforth and A. Provenzalle (Springer Verlag, Berlin,

2001), p. 403.
[4] H.M. Jaeger, C. Liu, S.R. Nagel, and T.A. Witten, Europhys. Lett. **7**, 619 (1990); G.H. Ristow, F.-X. Riguidel, and D. Bideau, J. Phys. I **4**, 1161 (1994); F.-X. Riguidel, R. Jullien, G.H. Ristow, A. Hansen, and D. Bideau, *ibid.* **4**, 261 (1994); S. Dippel, G.G. Batrouni, and D.E. Wolf, Phys. Rev. E **56**, 3645 (1997); S. Dippel, G.G. Batrouni, and D.E. Wolf, *ibid.* **54**, 6845 (1996); L. Quartier, B. Andreotti, S. Douady, and A. Daerr, *ibid.* **62**, 8299 (2000).
[5] C. Ancey, P. Evesque, and P. Coussot, J. Phys. I **6**, 725 (1996).
[6] J.R. Smart and D.T. Leighton, Phys. Fluids A **1**, 52 (1993); K.P. Galvin, Y. Zhao, and R.H. Davis, Phys. Fluids **13**, 3108 (2001).
[7] M.W. Reeks and D. Hall, J. Aerosol Sci. **32**, 1 (2001).
[8] G. Parker, J. Fluid Mech. **89**, 127 (1978).
[9] J. Buffington, J. Hydraul. Res. **125**, 376 (1999).
[10] K.L. Johnson, *Contact Mechanics* (Cambridge University Press, Cambridge, 1985), p. 452.
[11] N. Maw, J.R. Barber, and J.N. Fawcett, Wear **1**, 101 (1976); N. Maw, J.R. Barber, and J.N. Fawcett, J. Lubr. Technol. **103**, 74 (1981); S. Foerster, M. Louge, H. Chang, and K. Allia, Phys. Fluids **6**, 1108 (1994).
[12] P.L. Wiberg and J.D. Smith, Water Resour. Res. **23**, 1471 (1987).
[13] C.-H. Ling, J. Hydraul. Res. **121**, 472 (1995).
[14] Y.-M. Chew and G. Parker, J. Hydraul. Res. **32**, 649 (1994).
[15] W.W. Willmarth and R.L. Enlow, J. Fluid Mech. **36**, 417 (1969); M.S. Howe, G.C. Lauchke, and J. Wang, *ibid.* **436**, 41 (2001).
[16] D.T. Gillespie, *Markov Processes, an Introduction for Physical Scientists* (Academic Press, San Diego, 1992); S.M. Ross and Simulation (Academic Press, San Diego, 1997).
[17] L. van Rijn, J. Hydraul. Res. **110**, 1431 (1985).
[18] C. Ancey, F. Bigillon, P. Frey, J. Lanier, and R. Ducret, Phys. Rev. E **66**, 036306 (2002).
[19] S.B. Pope, *Turbulent Flows* (Cambridge University Press, Cambridge, 2000), p. 771.
[20] I. Nezu and H. Nakagawa, *Turbulence in Open-Channel Flows* (Balkema, Rotterdam, 1993), p. 281.
[21] V.T. Chow, *Open-Channel Hydraulics* (McGraw Hill, New York, 1959).
[22] S.A. Morsi and A.J. Alexander, J. Fluid Mech. **55**, 193 (1972); R. Kurose and S. Kumori, *ibid.* **384**, 183 (1999).
[23] J. Sheridan, J.C. Lin, and D. Rockwell, J. Fluid Mech. **330**, 1 (1997).
[24] W.H. Graf, *Hydraulics of Sediment Transport* (Water Resources Publications, Littleton, 1984).
[25] R.A. Bagnold, Proc. R. Soc. London, Ser. A **249**, 235 (1956).
[26] A.N. Papanicolaou, S.P. Dipla, N. Evaggelopoulos, and S. Fotopoulos, J. Hydraul. Res. **128**, 369 (2002).
[27] G. Parker, C. Paola, and S. Leclair, J. Hydraul. Res. **126**, 818 (2000).
[28] I.V. Derevich, Int. J. Heat Mass Transf. **43**, 3709 (2000); E. Peirano and J.-P. Minier, Phys. Rev. E **65**, 046301 (2002).